Research Article Vol. 31, No. 14 / 3 Jul 2023 / Optics Express 23419
Optics EXPRESS

15-μJ picosecond hollow-core-fiber-feedback optical parametric oscillator

YUDI WU, QIANG FU, SIJING LIANG, FRANCESCO POLETTI, DAVID J. RICHARDSON, AND LIN XU*

Optoelectronics Research Centre, University of Southampton, Southampton, SO17 1BJ, UK
**l.xu@soton.ac.uk*

Abstract: We report a high-energy, picosecond, mid-infrared (MIR) optical parametric oscillator (OPO), in which a length of hollow-core-fiber (HCF) is employed to enable operation at 1-MHz repetition rate in a compact cavity format. The OPO is synchronously pumped by an ytterbium-doped-fiber (YDF) master-oscillator-power-amplifier (MOPA) system, seeded by a 1040-nm gain-switched laser diode (GSLD). Using periodically poled lithium niobate (PPLN) as the nonlinear crystal, the OPO generates signal and idler beams with tunable wavelengths in the range of 1329–1641 nm and 2841–4790 nm, respectively. The OPO provides 137-ps pulses with a maximum signal energy of 10.05 μJ at 1600 nm and a maximum idler energy of 5.13 μJ at 2967 nm. This, to the best of our knowledge, represents the highest energy MIR pulses, as well as the highest total converted pulse energy (15.18 μJ), ever achieved from a fiber laser pumped picosecond OPO.

1. Introduction

Ultrashort-pulsed mid-infrared (MIR) lasers are of great interest in a diverse range of applications such as spectroscopy, material processing, free-space communications, and medical treatments [1–4]. Specifically in medical applications, picosecond MIR sources are very attractive for high-precision biological tissue ablation [5–7]. Synchronously pumped optical parametric oscillators (SPOPOs) are commonly used to service these applications through frequency conversion of readily available near-infrared (NIR) pulses to the MIR. However, SPOPOs have a requirement for temporal synchronization between the pump and the resonated signal to maintain stable operation for ultrashort pulses. Hence, a long cavity length is required when pumped with high-energy pulses at a low repetition rate. For example, a 3-m-long cavity is required for SPOPO to operate at a 100 MHz repetition rate [8], whereas a cavity length of 8.16 m is needed to achieve a repetition rate of 36.7 MHz [9]. It can be seen that if the repetition rate is further reduced, then conventional free-space SPOPOs would require a very long and complex cavity design and impose great physical and practical issues.

One method to overcome this practical difficulty of SPOPOs is to use a piece of optical fiber inside the OPO cavity as a delay line to allow synchronous pumping at low repetition rates whilst realizing a compact cavity design [10–12]. Such a cavity is known as a fiber-feedback cavity. Previously, we reported a fiber-feedback OPO using a ~300-m length of hollow-core fiber (HCF) in the cavity as the intracavity delay line and showed the ultralow nonlinearity of the HCF significantly improved the power scalability of the OPO compared to a traditional solid-core fiber-feedback OPO [13]. A maximum MIR pulse energy of 1.5 μJ at 2950 nm was achieved from the HCF fiber-feedback OPO with further power scaling being limited by the ytterbium-doped-fiber (YDF) master-oscillator-power amplifier (MOPA) pump source, which exhibited strong nonlinear spectral broadening at pump powers over 7.3 W. Here we demonstrate the development of a new MOPA system that provides a maximum pump power of 33.8 W by

#494037 https://doi.org/10.1364/OE.494037
Journal © 2023 Received 25 Apr 2023; revised 15 Jun 2023; accepted 15 Jun 2023; published 28 Jun 2023

Optics EXPRESS

reducing the nonlinearities in the fiber amplifiers. Using this upgraded MOPA source as the pump, we explored the power scaling of a HCF fiber-feedback OPO based on a periodically poled lithium niobate (PPLN) crystal and synchronously pumped at 1-MHz repetition rate. Using this system, a maximum overall pulse energy of over 15 µJ was realized, for the first time. In addition, wavelength tunability of the HCF fiber-feedback OPO has been expanded by using PPLN crystals with different poled grating periods to generate signals and idlers with wavelength ranges of 1329–1641 nm and 2841–4790 nm respectively, significantly pushing the MIR wavelengths beyond the previously reported 3563 nm. MIR pulse energies at 2967-nm up to 5.13 µJ and NIR pulse energies at 1600-nm up to 10.05 µJ were achieved. This, to the best of our knowledge is the highest energy MIR pulses as well as the highest total converted pulse energy (15.18 µJ) achieved from a fiber laser pumped picosecond SPOPO. Furthermore, systematic studies of pump acceptance bandwidth for the widely-tunable OPO and its influence on the OPO power performance at different wavelength has been carried out both theoretically and experimentally.

2. Experimental setup

The OPO pump source is an in-house-built fully polarization-maintaining (PM) YDF MOPA system, seeded by a 1040-nm gain-switched laser-diode (GSLD), with a configuration similar to that reported in [13], but with slight modifications. The schematic setup of the MOPA system is illustrated in Fig. 1. The GSLD (1064CHP, 3SPhotonics) seed laser was operated at a 64.0-MHz repetition rate, producing 137-ps pulses at 1040 nm, with a 0.37-mW average output power. Aside from the GSLD, the MOPA comprised four YDF amplifier stages and an electro-optic modulator (EOM). The MOPA incorporates core-pumped PM YDFs (PM-YDF-5/130-VIII, Nufern) with a 5-µm core diameter in the first and the second amplifier stages, a cladding-pumped PM YDF (PMLA-YDF-10/125-VIII, Nufern) with an 11-µm core and 125-µm cladding diameter in the third stage, and a backwards cladding-pumped PM YDF (PMLA-YDF-30/250-HI-8, Coherent) with a 30-µm core and 250-µm cladding diameter in the fourth stage. The 30/250-µm YDF in the fourth amplifier stage replaced the previously used 25/250-µm fiber in [10] to reduce the nonlinearities and hence allowed the power scaling of the MOPA system. An in-house fabricated fiber taper was implemented between the third and fourth stages, where a length of passive fibre with core/cladding diameter of 30/250 µm was tapered down using an automated glass processor (GPX-3000, Vytran) to have a smaller core size with a MFD matching that of the YDF used in the third-stage amplifier.

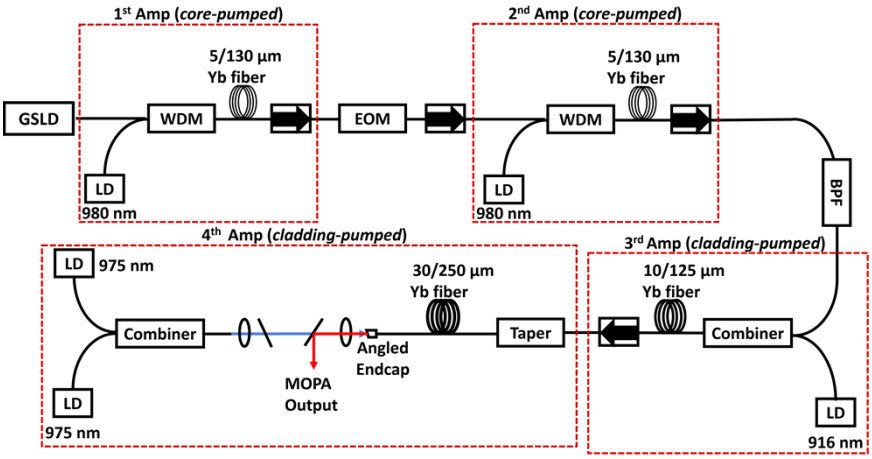

Fig. 1. Schematic of the MOPA pump system. GSLD: gain-switched LD; WDM: wavelength division multiplexer; LD: pump LD; EOM: electro-optic modulator; BPF: bandpass filter.

Optics EXPRESS

The pump laser diodes (LDs) used in the MOPA amplification stages were 980-nm single-mode LDs with 200-mW launch power in the first and second stages, a 916-nm multi-mode LD with 1.5-W launch power in the third stage, and two 975-nm wavelength-stabilized multi-mode LDs providing 80-W total launch power in the fourth stage, respectively. The core-pumped YDFs used in the first and second-stage amplifiers had lengths of 80 cm and 3 m respectively, and the length of cladding-pumped YDF used in the third stage amplifier is 1.25 m. The 30/250-μm large-mode-area (LMA) YDF used in the fourth stage amplifier had a high cladding-pump absorption of 7.2 dB/m, hence a short length of 1.8 m was chosen to provide a suitable balance between high-power efficiency and low nonlinearity. This LMA YDF can support 4 spatial modes, hence the fiber is coiled with a diameter of 50-mm to enhance the leakage loss of the higher order modes whilst maintaining low loss for the fundamental mode allowing single mode operation. An EOM was inserted between the first and second amplification stages and used as a pulse picker to reduce the pulse repetition rate down to 1 MHz. A 1040-nm fiber bandpass filter (BPF) was inserted after the second stage to reduce the buildup of amplified spontaneous emission (ASE) in the MOPA system. The power-scaled MOPA provided an average output power of up to 33.7 W with a slope efficiency of 60.1% (Fig. 2(a)) in a linearly polarized beam with a diffraction-limited beam quality (M2 ~ 1.02).

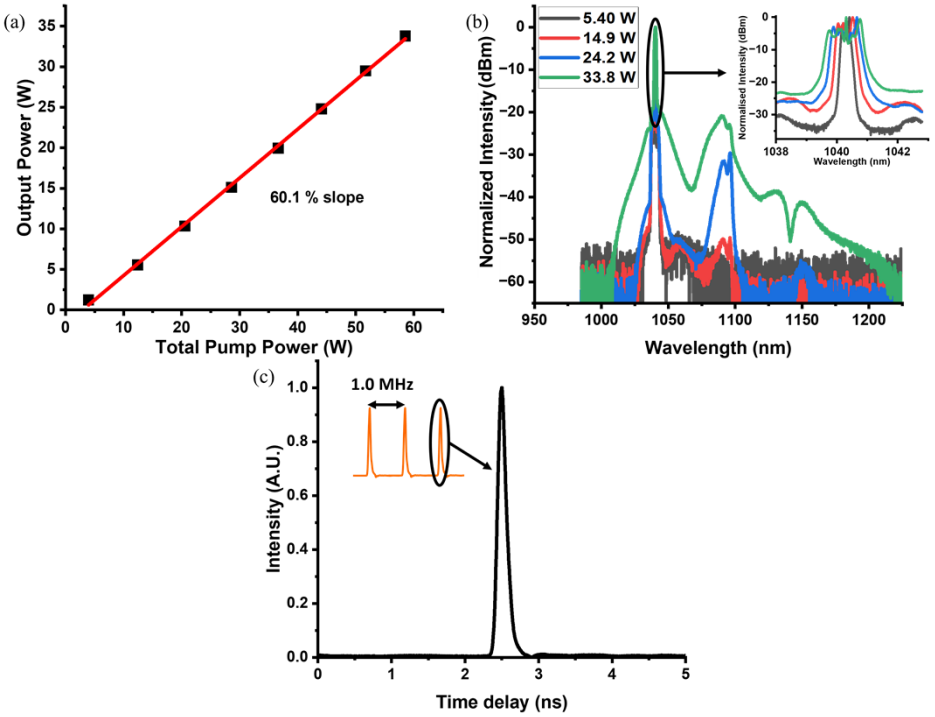

Fig. 2. Graphs showing the MOPA performance: (a) optical power with a linear fit against pump power for the 4th amplifier, (b) optical spectra at different powers (inset shows spectral peak with a higher resolution) and (c) optical pulse at the maximum power (inset shows the 1-MHz pulse train).

Figure 2(b) shows the output spectrum at different powers from the MOPA. Self-phase-modulation (SPM) induced spectral broadening was observed at high peak powers (inset of Fig. 2(b)). At 33.8-W average power, the 10-dB spectral linewidth was 1.3 nm, which is within the estimated pump acceptance bandwidth of the nonlinear crystal of the OPO (1.32-nm at 1600-nm wavelength and 40-mm crystal length). Note that a 10-dB spectral linewidth was

Optics EXPRESS

used for the MOPA spectra exhibiting a multipeak structure due to SPM, which covers >80% of the full power/energy within that wavelength range. The peaks in the spectrum at 1091 nm and 1150 nm (Fig. 2(b)) arise from Raman frequency shifting that occurred due to the high peak powers in the fourth-stage amplifier. Further increase in the MOPA output power would not only increase the main spectral width at the 1040-nm peak beyond the pump acceptance bandwidth due to SPM, but also increase the Raman power significantly and therefore reduce the energy in the main 1040-nm peak. Both these unwanted nonlinear effects would reduce the OPO's conversion efficiency. The MOPA output pulse at the maximum power was measured using a 32-GHz-bandwidth photo-detector (83440D, Agilent) and a 20-GHz-bandwidth digital communication analyzer (Infiniium 86100C, Agilent), showing a pulse duration of 137 ps as seen in Fig. 2(c), which is similar to that of the GSLD seed. The MOPA was operated at the maximum power and a power attenuator, consisting of a pair of half-wave plates (HWP in Fig. 3) and a polarizing beam-splitter (PBS in Fig. 3), was employed to control the OPO's pump power while maintaining the same pump spectra.

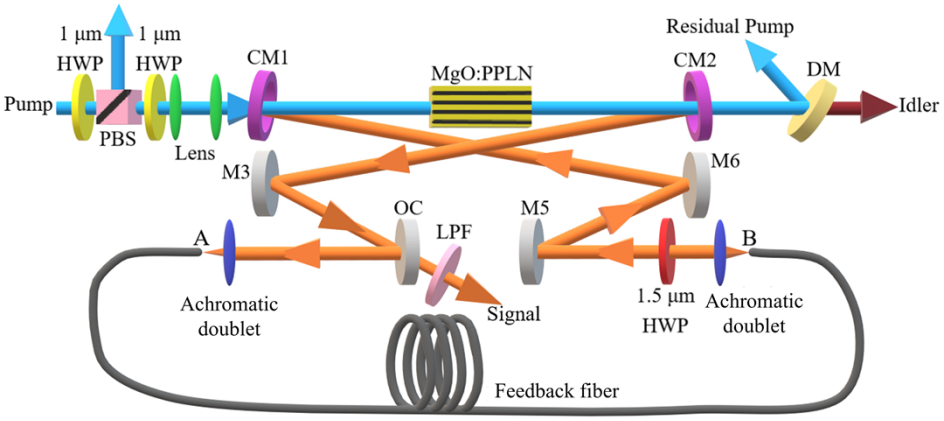

Fig. 3. Schematic of the OPO. HWP: Half-waveplate; PBS: polarizing beam-splitter cube; CM1, CM2: concave mirrors; MgO:PPLN: 5% MgO doped periodically poled lithium niobate, M3, M5 and M6: plane mirrors; OC: 90% output coupler; DM: 45° Dichroic mirror; LPF: Long pass filter.

The OPO was of a signal-resonant ring-cavity design, consisting of two concave mirrors, two plane mirrors, an optical fiber, and a periodically poled lithium niobate (PPLN) nonlinear crystal. A schematic of the OPO cavity is presented in Fig. 3. Both concave mirrors (CM1 and CM2 in Fig. 3) had a radius of curvature of 250 mm and were of high reflectivity (>99%) at signal wavelengths (1.3–1.7 μm) and provided ~ 81% transmission at the pump wavelength (1 μm) and had a transmission of < 81% across the entire range of OPO idler wavelengths (3–5 μm). The plane mirrors (M3, M5 and M6 in Fig. 3) were silver mirrors of high reflectivity (>99%) at all the wavelengths involved (i.e., pump, signal and idler). An output coupler of 90% signal transmission (OC in Fig. 3) was used to allow signal light to be coupled out of the cavity. A long pass filter of < 86% transmission at signal wavelengths and a 45° dichroic mirror of < 68.8% transmission at idler wavelengths were used to filter out the residual pump during signal and idler measurements respectively. The total free-space length of the OPO cavity was 1.58 m.

To match the pump to the signal cavity mode, which had a calculated beam radius (using standard ABCD matrices of the ring cavity for a stable resonator) of 283 μm at the center of the PPLN crystal, the MOPA output beam was focused down to a measured beam radius of 287 μm with a pair of plano-convex lenses of 100-mm and 50-mm focal length. Note that due to physical space restrictions in our set up, and lack of ready access to a suitable single lens solution, a

Optics EXPRESS

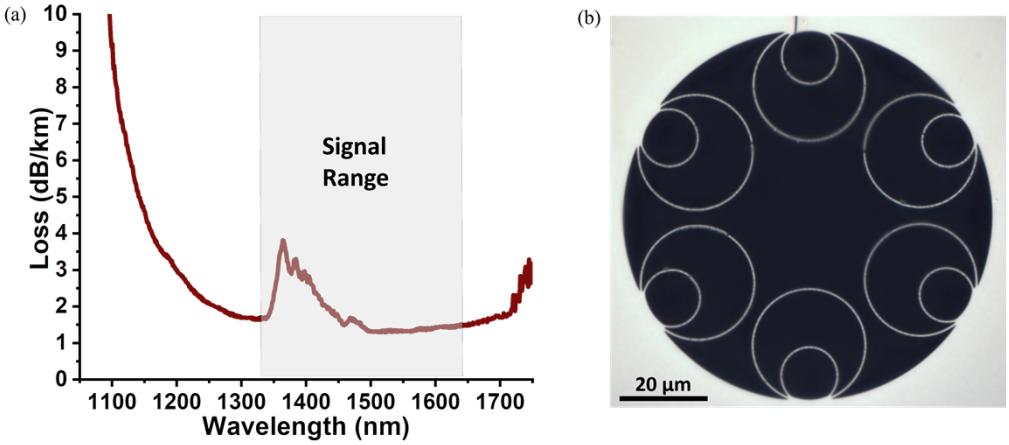

Fig. 4. Graph showing the (a) cutback plot of the HCF fiber used in the fiber-feedback OPO cavity (1.35-nm resolution) and (b) the HCF fiber cross-section.

combination of two available lenses were used to focus the pump beam to the exact position and with the specific beam waist required. The 40-mm-long PPLN crystal (MOPO1-1.0-40, Covesion), had 5 poled gratings with periods ranging from 29.52–31.59 µm in steps of 0.5 µm, providing the phase matching needed for the OPO to generate signals and idlers at wavelengths in the range of 1472 –1641 nm and 2841–3556 nm, respectively. The crystal was mounted in an oven that allowed temperature tuning from 20 to 200 °C. In further experiments, a 50-mm-long PPLN crystal (MOPO2-1.0-50, Covesion) with 7 poled gratings with periods ranging from 28.5–25.5 µm in steps of 0.5 µm was used to show the wavelength tuning capability for signal and idler wavelength ranges of 1329–1429 nm and 3823–4791 nm respectively.

The feedback fiber used was an in-house-fabricated HCF similar to that used in our previously reported system [13], which has a nested anti-resonant nodeless fiber (NANF) geometry [14]. The cross-section of the NANF is presented in Fig. 4(b). The light was confined to the central void by the presence of the 6 non-contacting nested tube elements through coherent antiresonant reflection as determined by the thickness of the membrane elements [15]. The NANF fiber used here was of 33.5-µm core diameter and was single mode with < 4 dB/km loss at 1300 nm – 1700nm (signal), as shown in the cutback loss measurement plot in Fig. 4(a). A 298-m length of HCF was chosen for the OPO to match with the 1-MHz pump repetition rate (this takes into account the free-space component of the cavity and assumes a group index close to 1). The synchronization between the recirculating signal pulses and the pump pulses was optimized by adjusting the positions of the input and output ends of the HCF which were mounted on translational stages with 2-cm travel distance in the longitudinal direction. In addition to the low nonlinearity, the HCF had an estimated group velocity dispersion (GVD) of -3.5 fs^2/mm at 1550 nm, about 6 times smaller than a standard solid-core SMF-28 (-23 fs^2/mm), helping to avoid distortion and the increase in the signal pulse duration by a factor of ~1.5 observed when using an SMF-28 feedback-fiber [13]. The GVD of the HCF was estimated from numerical simulation of the HCF based on its cross-sectional structure, similarly to that provided in [16]. Also, we experienced not issues with pump synchronization as the signal wavelength was tuned due to the low, spectrally-flat GVD properties of the NANF HCF [16] and the long (137 ps) pump pulses used. Thus, an HCF feedback-fiber is highly beneficial in realizing such short-pulsed OPOs. At points A and B of the OPO cavity (Fig. 3), achromatic doublet lenses of 25-mm focal length were used to couple the signal in and out of the feedback fiber while matching the cavity mode. Antiresonant HCFs have previously been demonstrated to provide good capability in terms of

Optics EXPRESS

maintaining polarization purity [17]. Although we did not fully characterize the polarization maintaining properties of the HCF used in our experiment we found that placing and suitably adjusting a half-wave plate for the resonant signals after the HCF was an effective way to achieve high conversion efficiency for the OPO operating under such high gain conditions.

For the idler measurements, a 45° dichroic mirror (DM in Fig. 3) of high reflectivity at 1 µm and 68.8% transmission at 3 µm, was placed after the OPO cavity to filter out the residual pump light. A long-pass filter of 0.002% transmission at 1 µm and 86.1% transmission at 1.5 µm, was placed after the output coupler to allow signal measurements.

3. Results and discussions

OPO operation was observed at a pump threshold of 4.9-W average power using a 30.49-µm PPLN grating at an oven temperature of 100 °C. The idler output average power (black), taking into account the loss of CM2 and DM, the signal output average power (red) and the total converted power (i.e. sum of signal and idler power) with respect to different pump powers are shown in Fig. 5(a). In theory the full idler power could be accessible if CM2 and DM had an idler transmission of 100%. The idler power increased linearly with respect to the pump power at a slope efficiency of 22.1% up to a maximum power of 5.13 W, and the signal power also increased linearly with respect to the pump power with a slope efficiency of 44.1% up to a maximum power of 10.05 W. This corresponds to an overall slope efficiency of 66.2% and maximum total converted power of 15.18 W. The total power conversion efficiency at the maximum pump power reaching the PPLN was calculated to be 55.5% at 27.35 W maximum pump power (81% of the incident 33.8 W pump power). The corresponding maximum signal and idler pulse energies (peak powers) are 10.05 µJ (72.3 kW) and 5.13 µJ (36.9 kW), respectively. This is over 3 times the maximum achieved in previously reported results [13]. To the best of our knowledge, these results represent the highest energy pulses (both MIR and total converted) achieved from a fiber laser pumped picosecond OPO.

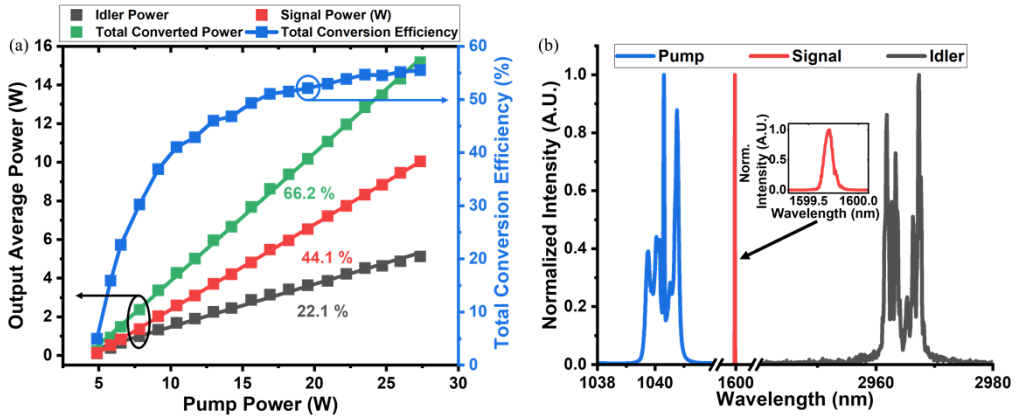

Fig. 5. Graphs showing: a) the OPO's average idler power with linear fit (black), average signal power with linear fit (red), total converted power with linear fit (green) and conversion efficiency (blue dots) against pump power (the blue line is a guide for the eye); b) the spectra of signal (red) and idler (black) from the OPO, and the pump spectrum (blue) for comparison. The inset shows the magnified signal spectrum.

The spectrum of the resonated signal from the OC was measured with a spectrum analyzer (OSA) (AQ6375, Yokogawa, 0.05-nm resolution) and is shown in Fig. 5(b). The central wavelength of the signal generated is 1599.7 nm with a full width at half maximum (FWHM) of 0.09 nm. The corresponding idler spectrum, measured with an OSA (721 series, Bristol

Optics EXPRESS

instruments, 4-GHz resolution), is also presented in Fig. 5(b). The central idler wavelength generated is 2967 nm with a spectral width of 7.49 nm. The multipeak nature of the idler spectrum and much wider spectral width originates from the transfer of the pump spectrum (blue spectrum in Fig. 5(b)) through the parametric process - similarly to that reported and described in the previous studies on parametric transfer [18–20].

The coupling efficiency of the intracavity signal into the HCF feedback fiber was also measured. The power reflected from a pellicle beam splitter of 5% signal reflectivity placed at the output end of the fiber was measured and from this the total power leaving the fiber could be deduced. The power of the incident signal at the HCF input can be determined from the power measured after the OC. The signal coupling efficiency into the HCF feedback fiber can then be calculated from the signal powers at the fiber input and the fiber output, taking into account the HCF propagation loss. A 46% coupling efficiency was calculated for an output power of 0.66 W, which reduced to 10% at maximum power due to the degradation in beam quality as the power is increased (see below).

To characterize the wavelength tunability of the OPO, different PPLN grating periods of the MOPO1-1.0-40 and MOPO2-1.0-50 crystals were used at different oven temperatures, and the output signal and idler spectra were measured. A seamless wavelength tuning of the signal and idler output across the ranges of 1329–1641 nm and 2841–4791 nm, respectively, were achieved. Examples of several spectra with different central wavelengths are shown in Fig. 6(a). Maximum output powers for the signal and idler at different wavelengths were characterized and are presented in Fig. 6(b). The output powers reach their maximum for the signal and idler at wavelengths of around 1600 nm and 3000 nm, respectively, and they decrease at both sides of the wavelength tuning range.

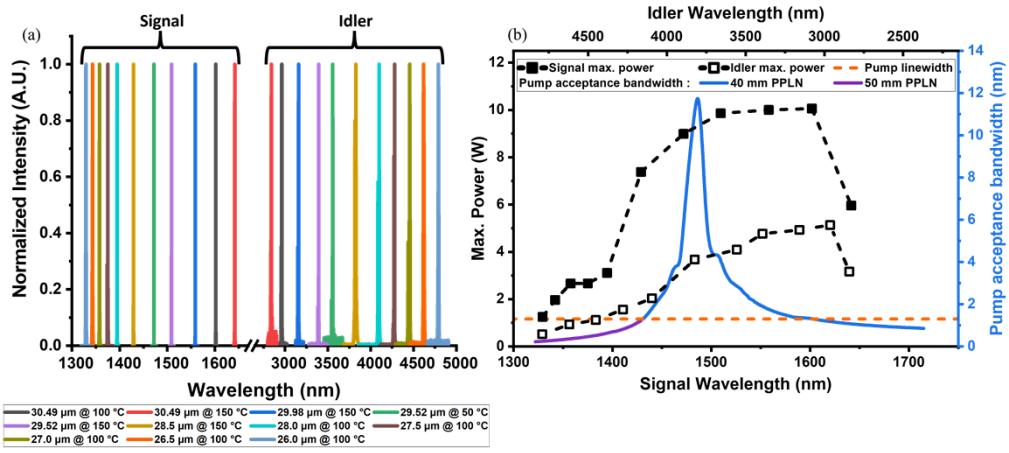

Fig. 6. Graphs showing: a) tunability of the signal and idler, and (b) the corresponding maximum output powers and calculated pump acceptance bandwidths. The orange dashed horizontal line marks the 1.3-nm spectral width of the pump (with the right vertical axis).

To understand and explain the power change, the pump spectral acceptance bandwidth for the OPO using 40 mm/50 mm PPLN crystals and operating at these wavelengths was calculated [21] and is plotted in Fig. 6(b). The pump acceptance bandwidth varies significantly with respect to the signal/idler wavelength due to the wavelength dependent dispersion of the PPLN crystals. A dashed horizontal line marking the real pump spectral linewidth is also shown in the figure. It can be found that the rapid power drop of signal (idler) at >1600 nm (<2967 nm) was due to the reduction of the pump acceptance bandwidth with respect to the actual pump bandwidth. In the wavelength range of 1429–1510 nm (signal) and 3393–3823 nm (idler), the maximum power

Optics EXPRESS

exhibits a slow decrease, which is likely due to the slightly increased loss of the HCF due to water vapor absorption at these wavelengths. A rapid power decrease can be seen for the wavelengths of signal (idler) tuning from 1429–1329 nm (3823-4791 nm) where the theoretical pump acceptance bandwidth becomes smaller than the pump bandwidth. One possible method to overcome this problem is to further reduce the spectral width of the pump source by further reducing the MOPA nonlinearities, e.g. using a final-stage Yb gain fiber with an even bigger core size to reduce the pulse intensity in the fiber or a larger cladding-pump absorption to shorten the fiber length, and hence further improve the power scalability over the entire wavelength range. However, such a setup would require more complex high-order mode suppression or water cooling of the gain fiber, which would further complicate the setup. Alternatively, a PPLN crystal with a shorter length could be used to increase the pump acceptance bandwidth, however, this would result in a lower optical parametric gain and reduce the OPO efficiency. Further investigations on power-scaling of the OPO over the entire wavelength range are currently underway.

The signal and idler power stability at the maximum output was measured over the course of 1 hour (Fig. 7(a)), with corresponding RMS values of 1.3% and 1.6% respectively. The good power stability of the OPO is attributed to the stable pump MOPA source, high-gain operation of the OPO and robust cavity design.

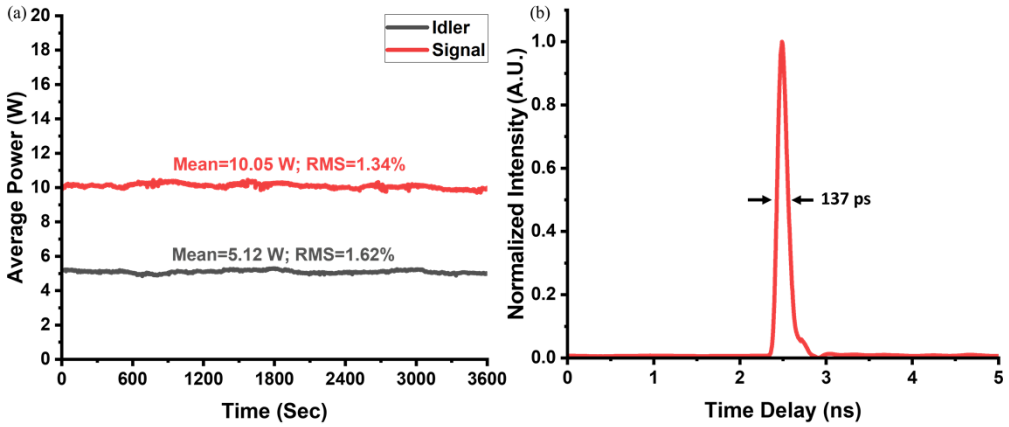

Fig. 7. Graphs showing a) power stability of the OPO's signal (red) and idler (black) at maximum output over a 1-hour time frame, and b) the OPO's output signal pulse.

The output signal pulse duration of the OPO was also measured and is shown in Fig. 7(b). The signal pulses maintained the same duration as that of the pump (137 ps) due to the low intracavity nonlinearity and dispersion. Note that the output idler pulses were not measured due to a lack of suitable instrumentation, however we would expect those to also have a similar duration to that of the pump.

The signal and idler beam quality were measured using a pyroelectric scanning profiler at low (1.4 W Fig. 8(a)) and 1.0 W Fig. 8(c), respectively) and high (10.05 W Fig. 8(b) and 5.13 W Fig. 8(d) respectively) output powers. At low output powers, a beam quality of $M_x^2 = 1.34$ and $M_y^2 = 1.37$ for the signal, and $M_x^2 = 1.90$ and $M_y^2 = 1.94$ for the idler were obtained. The beam quality degraded with increased output power to $M_x^2 = 2.92$ and $M_y^2 = 3.26$ for the signal and $M_x^2 = 3.32$ and $M_y^2 = 3.77$ for the idler at the maximum output power. The degradation in beam quality at high powers is likely due to the non-uniformity of pump depletion across the beam at the high pump intensity and high parametric gain. Other methods, such as difference frequency generation (DFG) and optical parametric amplification (OPA), have been demonstrated to enable MIR laser sources with relatively good beam quality [22–24]. However, the requirement of two laser sources increases the complexity and cost of the setup. Furthermore, the wavelength

Optics EXPRESS

tunability of the system is generally limited by the laser sources. The HCF fiber-feedback OPO represents a promising solution for the development of high-energy short-pulsed tunable lasers. Further work to optimize the HCF fiber-feedback OPO's output beam quality at high power using different cavity designs and mirrors to increase the cavity mode beam waist and reduce pump intensity inside the PPLN crystal is currently underway.

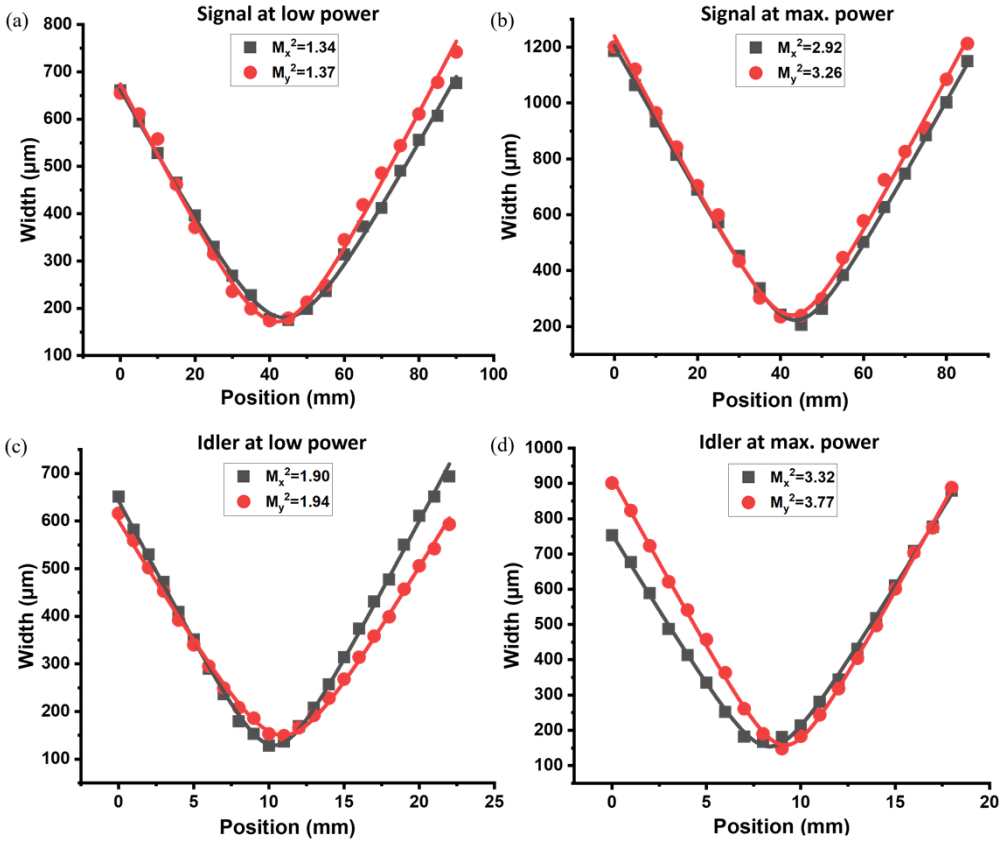

Fig. 8. Beam quality measurements of signal at (a) low power and (b) at maximum power, and idler at (c) low power and (d) maximum power.

4. Conclusion

In conclusion, we have demonstrated a 1-MHz repetition-rate, compact picosecond-pulsed HCF fiber-feedback OPO based on PPLN providing MIR pulse energies up to 5.13 μJ and 1600 nm NIR pulse energies up to 10.05 μJ. This, to the best of our knowledge is the highest energy MIR pulses and total converted pulse energy (15.18 μJ) achieved from a fiber laser pumped picosecond SPOPO. Using PPLNs with different poling periods for the OPO, widely tunable signal and idler wavelength ranges of 1329–1641 nm and 2841–4790 nm, respectively, were realized. The variance of pump acceptance bandwidth with respect to the wavelength tuning and its effect on the output power of the OPO were also investigated. When the pump acceptance bandwidth becomes smaller than the pump bandwidth, a significant drop in OPO output power was observed. This was observed for signal (idler) wavelengths within 1429–1329 nm (3823–4791 nm) and wavelengths >1600 nm (2967 nm). Further power scaling of the OPO is still possible if the nonlinearities in the MOPA pump system can be further reduced e.g. through using a final-stage

Optics EXPRESS

Yb gain fiber with a larger cladding-pump absorption such that a shorter length of gain fiber could be used. However, such a setup would require water cooling of the gain fiber which would further complicate the setup.

Funding. Engineering and Physical Sciences Research Council (EP/P027644/1, EP/P030181/1, EP/T020997/1, EP/V038036/1).

Acknowledgements. The authors would like to thank Emeritus professor David Shepherd from the Optoelectronics Research Centre for useful discussions. The authors also thank Dr. Dong Wu for her help in fabricating the fiber taper.

Disclosures. The authors declare no conflicts of interest.

Data Availability. Data underlying the results presented in this paper are available in Ref. [25].

References

1. M. W. Sigrist, "Mid-infrared laser-spectroscopic sensing of chemical species," J. Adv. Res. **6**(3), 529–533 (2015).
2. R. Knappe, H. Haloui, A. Seifert, A. Weis, and A. Nebel, "Scaling ablation rates for picosecond lasers using burst micromachining," Proc. SPIE **7585**, 75850H (2010).
3. Y. Su, W. Wang, X. Hu, H. Hu, X. Huang, Y. Wang, J. Si, X. Xie, B. Han, H. Feng, Q. Hao, G. Zhu, T. Duan, and W. Zhao, "10 Gbps DPSK transmission over free-space link in the mid-infrared," Opt. Express **26**(26), 34515–34528 (2018).
4. M. Mackanos, D. Simanovskii, K. Schriver, M. Hutson, C. Contag, J. Kozub, and E. Jansen, "Pulse-Duration-Dependent Mid-Infrared Laser Ablation for Biological Applications," IEEE J. Sel. Top. Quantum Electron. **18**(4), 1514–1522 (2012).
5. A. Krutilin, S. Maier, R. Schuster, S. Kruber, M. Kwiatkowski, W. D. Robertson, N.-O. Hansen, R. J. D. Miller, and H. Schlüter, "Sampling of Tissues with Laser Ablation for Proteomics: Comparison of Picosecond Infrared Laser and Microsecond Infrared Laser," J. Proteome Res. **18**(3), 1451–1457 (2019).
6. R. Battle, D. Simon, Y. Xiang, T. Runcorn, R. A. Battle, D. Simon, Y. Xiang, K. Robinson, H. Timothy, R. T. Murray, J. R. Taylor, and Z. Takats, "High resolution mass spectrometry imaging using 3 micron laser ablation," Proc. SPIE **12377**, 1237706 (2023).
7. K. Franjic, M. L. Cowan, D. Kraemer, and R. J. D. Miller, "Laser selective cutting of biological tissues by impulsive heat deposition through ultrafast vibrational excitations," Opt. Express **17**(25), 22937–22959 (2009).
8. Q. Fu, L. Xu, S. Liang, P. C. Shardlow, D. P. Shardlow, S. Alam, and D. J. Richardson, "High-average-power picosecond mid-infrared OP-GaAs OPO," Opt. Express **28**(4), 5741–5748 (2020).
9. C. W. Rudy, A. Marandi, K. A. Ingold, S. J. Wolf, K. L. Vodopyanov, R. L. Byer, L. Yang, P. Wan, and J. Liu, "Sub-50 fs pulses around 2070nm from a synchronously-pumped, degenerate OPO," Opt. Express **20**(25), 27589–27595 (2012).
10. T. Südmeyer, E. Innerhofer, F. Brunner, R. Paschotta, T. Usami, H. Ito, S. Kurimura, K. Kitamura, D. C. Hanna, and U. Keller, "High-power femtosecond fiber-feedback optical parametric oscillator based on periodically poled stoichiometric $LiTaO_3$," Opt. Lett. **29**(10), 1111–1113 (2004).
11. F. Kienle, P. S. Teh, S. Alam, C. B. E. Gawith, D. C. Hanna, D. J. Richardson, and D. P. Shepherd, "Compact, high-pulse-energy, picosecond optical parametric oscillator," Opt. Lett. **35**(21), 3580–3582 (2010).
12. T. Steinle, F. Mörz, A. Steinmann, and H. Giessen, "Ultra-stable high average power femtosecond laser system tunable from 1.33 to 20 µm," Opt. Lett. **41**(21), 4863–4866 (2016).
13. Y. Wu, S. Liang, Q. Fu, T. D. Bradley, F. Poletti, D. J. Richardson, and L. Xu, "High-energy, mid-IR, picosecond fiber-feedback optical parametric oscillator," Opt. Lett. **47**(14), 3600–3603 (2022).
14. F. Poletti, "Nested antiresonant nodeless hollow core fiber," Opt. Express **22**(20), 23807–23828 (2014).
15. G. A. Sanders, A. A. Taranta, C. Narayanan, E. N. Fokoua, S. A. Mousavi, L. K. Strandjord, M. Smiciklas, T. D. Bradley, J. Hayes, G. T. Jasion, and T. Qiu, "Hollow-core resonator fiber optic gyroscope using nodeless anti-resonant fiber," Opt. Lett. **46**(1), 46–49 (2021).
16. H. C. H. Mulvad, S. Abokhamis Mousavi, V. Zuba, H. Sakr, T. D. Bradley, J. R. Hayes, G. T. Jasion, E. Numkam Fokoua, A. Taranta, S.-U. Alam, D. J. Richardson, and F. Poletti, "Kilowatt-average-power single-mode laser light transmission over kilometre-scale hollow-core fibre," Nat. Photonics **16**(6), 448–453 (2022).
17. A. Taranta, E. Numkam Fokoua, S. Abokhamis Mousavi, J. R. Hayes, T. D. Bradley, G. T. Jasion, and F. Poletti, "Exceptional polarization purity in antiresonant hollow-core optical fibres," Nat. Photonics **14**(8), 504–510 (2020).
18. J. Prawiharjo, H. S. S. Hung, D. C. Hanna, and D. P. Shepherd, "Theoretical and numerical investigations of parametric transfer via difference-frequency generation for indirect mid-infrared pulse shaping," J. Opt. Soc. Am. B **24**(4), 895–905 (2007).
19. J. Prawiharjo, H. S. S. Hung, D. C. Hanna, and D. P. Shepherd, "Numerical investigations of parametric transfer in synchronously pumped optical parametric oscillators for indirect mid-infrared pulse shaping," J. Opt. Soc. Am. B **24**(9), 2484–2493 (2007).
20. H. S. S. Hung, J. Prawiharjo, N. K. Daga, D. C. Hanna, and D. P. Shepherd, "Experimental investigation of parametric transfer in synchronously pumped optical parametric oscillators," J. Opt. Soc. Am. B **24**(12), 2998–3006 (2007).
21. M.H. Dunn and M. Ebrahim-Zadeh, "Optical parametric oscillators," OSA Handbook of Optics, 22-1 (OSA, 2000), pp. 61–82.

Optics EXPRESS

22. L. Xu, H.-Y. Chan, S. Alam, D. J. Richardson, and D. P. Shepherd, "High-energy, near- and mid-IR picosecond pulses generated by a fiber-MOPA-pumped optical parametric generator and amplifier," Opt. Express **23**(10), 12613–12618 (2015).
23. R. T. Murray, T. H. Runcorn, S. Guha, and J. R. Taylor, "High average power parametric wavelength conversion at 3.31–3.48 μm in MgO:PPLN," Opt. Express **25**(6), 6421–6430 (2017).
24. P. Belden, D. W. Chen, and F. Di Teodoro, "Watt-level, gigahertz-linewidth difference-frequency generation in PPLN pumped by an nanosecond-pulse fiber laser source," Opt. Lett. **40**(6), 958–961 (2015).
25. Y. Wu, Q. Fu, S. Liang, F. Poletti, D. J. Richardson, and L. Xu, "Dataset supporting the article "15-μJ picosecond hollow-core-fiber-feedback optical parametric oscillator"," University of Southampton, 2023, https://doi.org/10.5258/SOTON/D2667